Eur. Phys. J. D **46**, 259–265 (2008)
DOI: 10.1140/epjd/e2007-00293-3

THE EUROPEAN PHYSICAL JOURNAL D

# Vibrational and rotational energy transfer of $CH^+$ in collisions with $^4$He and $^3$He

T. Stoecklin[1,a] and A. Voronin[2]

[1] Institut des Sciences Moléculaires, CNRS: UMR 5255, 351 cours de la Libération, 33405 Talence, France
[2] Russian Academy of Sciences, Institute of Chemical Physics, Chernogolovka, Moscow 142432, Russia

Received 5 July 2007
Published online 17 October 2007 – 

**Abstract.** A quantum mechanical investigation of vibrational and rotational energy transfer in cold and ultra cold collisions of $CH^+$ with $^3$He and $^4$He atoms is presented. Ab initio potential energy calculations are carried out at the BCCD(T) level and a global 3D potential energy surface is obtained using the Reproducing Kernel Hilbert Space (RKHS) method. Close coupling scattering calculations using this surface are performed at collision energy ranging from $10^{-6}$ to 2000 cm$^{-1}$. In the very low collision energy limit, the vibrational and rotational quenching cross sections of $CH^+$ in collisions with He are found to be of the same order of magnitude. This unusual result is attributed to the large angular anisotropy of the intermolecular potential and to the unusually small equilibrium value of the Jacobi $R$ coordinate of the He–$CH^+$ complex. As for the He–$N_2^+$ collision, we also find a strong isotope effect in the very low collision energy range which is analyzed in terms of scattering length and the differences between these two collisions are also discussed.

**PACS.** 34.20.Mq Potential energy surfaces for collisions – 34.50.-s Scattering of atoms and molecules – 34.50.Ez Rotational and vibrational energy transfer – 34.50.Pi State-to-state scattering analyses

## 1 Introduction

Many theoretical studies in the field of the production of ultra cold molecules are devoted to the understanding of collisional energy transfer [1] as it is now possible to experimentally study atom molecule interaction in this novel low temperature conditions. Such theoretical studies are also required to optimise the experimental cooling and trapping techniques of neutral [2–4] or ionic species [5,6]. Sympathetic cooling is currently used to cool charged diatomic molecules to tens of mK by coulomb interaction with laser cooled atomic ions in radio frequency ion traps. Photoassociative ionisation of heteronuclear diatomic molecules [7] is also used to produce ultra cold diatomic ions in magneto optical traps. However, cooling molecular ions both translationally and internally still remains a formidable task. Also, the understanding of the internal energy transfer of translationally cold diatomic ions in collisions with cold buffer gas such as $^3$He and $^4$He is both of theoretical and experimental interest.

For many of these atom diatom collisions, the probability of collisional energy transfer is very large at temperatures near zero Kelvin and small perturbations of the potential or variations of the relative mass in this range of temperature may suppress or create new resonance patterns. In a recent work we compared the vibrational [8] and rotational [9] quenching of $N_2^+$ in collisions with $^3$He and $^4$He and found that they exhibit a strong isotope effect in the ultra cold regime. As this effect is not obtained for collisions involving the neutral form of $N_2$, it is then expected to be a consequence of both the attractive ion-induced dipole interaction and the deeper well associated with ionic species. One motivation of the present work is to check if such an effect is a general trend of collisions involving ionic molecules.

The thermalisation of the rotational levels of the molecules occurs at rate which is usually comparable to the rate for cooling the translational motion and the vast majority of the trapped molecules are in their rotational ground state. The thermalisation of the vibrational levels is instead much slower. It was however realized long ago that for ionic systems, the presence of the long range potential alters the threshold behavior of the elastic and inelastic cross sections. The probability of vibrational quenching was experimentally found [10] in this case to increase when the collision energy decreases which is in contrast with the energy dependence due to short range forces which control vibrational quenching of neutral systems.

In the present study we consider the collisions of $CH^+$ with both $^3$He and $^4$He. We choose this system because of its simplicity which allows computing the potential energy surface at a high level of accuracy and because of the possibility of comparing with the neutral He–CH system which was studied theoretically [11] by other teams. The methylidyne cation is on the other hand a key species

[a] e-mail: t.stoecklin@ism.u-bordeaux1.fr

of the carbon chemistry in diffuse interstellar molecular clouds [12] and the knowledge of the rotational energy transfer rate coefficients is needed to evaluate the molecular abundance of $CH^+$. In the present work we then first build a three-dimensional potential energy surface (PES) which is then used to study both vibrational and rotational energy transfer for this system.

The plan of this paper is as follows. Section 2 contains a description of our ab initio calculations. The details of the construction of an analytical potential energy surface for this system are also given in Section 2. In Section 3, the method and the parameters used to make the scattering calculations are briefly discussed. The results of the Close Coupling calculations are eventually presented and analysed in Section 4.

## 2 Potential energy surface for He–$CH^+$ system

### 2.1 Ab initio calculations

The ab initio potential energy points for the three-dimensional potential energy surface of the He–$CH^+$ electronic ground state were calculated using the coupled cluster method [BCCD(T)] with Brueckner orbitals [13], in the supermolecular approach. The augmented-cc-pVQZ basis set of Dunning [14] was employed and supplemented by a set of bond functions as defined by Tao and Pan [15]. The interaction energy was obtained as the difference between the energy of the He–$CH^+$ complex and the sum of the monomers energies of the He and $CH^+$. The counterpoise procedure [16] was used to correct the basis set superposition error (BSSE) for each molecular configurations. The ab initio energy points were computed for 733 geometries expressed in Jacobi coordinates $(r, R, \theta)$. The calculations were carried out for five $CH^+$ bond distances ($r$ = 1.80, 2.0, 2.13728, 2.40 and 2.70 $a_0$). The grid of intermolecular distances $R$ is ranging (in $a_0$) from 2 to 10 in steps of 0.5; from 10 to 15 in steps of 1 and is complemented by the two values 18.0 and 20.0 $a_0$. The grid of Jacobi angle $\theta$ is ranging from 0 to 180° in steps of 30°. These geometries cover the region around the minimum, the long-range and repulsive parts of the potential energy surface. All the calculations were performed using the MOLPRO packadge [17].

### 2.2 Fitting procedure

As in our previous studies dedicated to the He–$N_2$, He–$F_2$, He–HF, H–$N_2$ and He–$N_2^+$ collisions, an analytical form of the potential energy surface was obtained using a fitting procedure based on the RKHS approach [18]. Since the details of this method were already described in our previous works [19], only a brief description is outlined below. Within the framework of the RKHS method, the interaction energy is written as follows

$$V(R,r,\theta) = \sum_{i=1}^{N_R}\sum_{j=1}^{N_r}\sum_{k=1}^{N_\theta} a_{ijk} q^{2,3}(R_i,R) q^{2,3}(r_j,r) q_1(z_k,z) \quad (1)$$

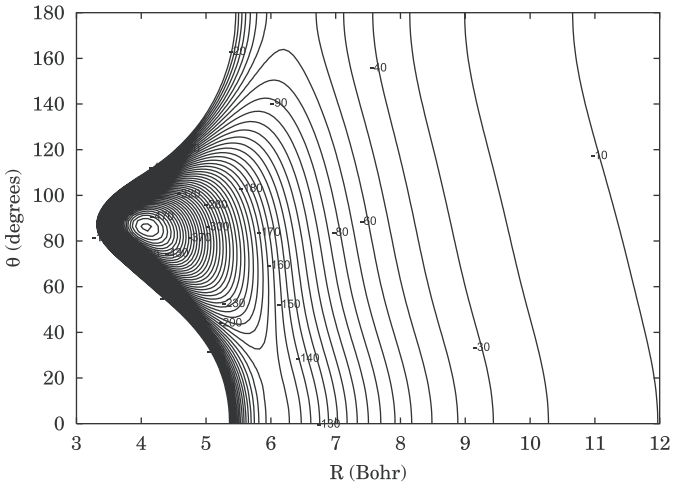


**Fig. 1.** Contour plot of the He–$CH^+$ potential energy surface in Jacobi coordinates. The contours are drawn by steps of 10 $cm^{-1}$ starting from –520 $cm^{-1}$. The $CH^+$ bond distance is fixed to 2.13728 Bohr.

where $z = (1-\cos\theta)/2, N_R, N_r, N_\theta$ denote the number of data points calculated along $R, r$ and $\theta$ Jacobi coordinates, and the $a_{ijk}$ are linear coefficients. The expressions of the one-dimensional reproducing kernel functions $q^{2,3}(R_i, R)$ which varies asymptotically in $1/R^4$ for large values of $R$ and of $q_1(z, z')$ are given in our previous works [8,19]. In order to check the quality of the long range part of our potential we compared its value $E = -4.41 \times 10^{-6}$ a.u. obtained for $R$ = 20 $a_0$, and $\theta$ = 90.0° with the value $V = -4.31 \times 10^{-6}$ a.u. obtained from the expression of the charge-induced dipole potential $V = -\alpha/2R^4$ using the experimental value of the polarisability of the He atom ($\alpha$ = 1.38 a.u.). The close agreement between these two values suggests that this level of calculation provides a good description of the long-range potential. The diatomic potential was obtained using a thin grid of ab initio points computed at the aug-cc-pV5Z level and a one-dimensional RKHS model. The well depth $D_e$ = 4.25 eV and the equilibrium distance $r_e$ = 2.13728 $a_0$ of the $CH^+$ diatomic potential are in good agreement with existing experimental data [20].

Figure 1 shows the contour plot of our RKHS potential energy surface for the He atom moving around the $CH^+$ molecule, the diatomic distance being set to its equilibrium value $r$ = 2.13728 $a_0$. The minimum of this figure is very close to the bent geometry ($R$ = 4.1 $a_0$, $r$ = 2.13128 $a_0$ and $\theta$ = 86.0°) of the minimum of the potential ($E = -513.573$ $cm^{-1}$). This is by far the deepest well among all the systems we treated previously as can be seen in Table 1 where we reported the geometry and the energy of several Van der Waals complexes. As can be seen in this table, the most striking difference with the geometries of all the other Van der Waals complexes are the large angular anisotropy and the equilibrium value of the Jacobi $R$ coordinate ($R$ = 4.1 $a_0$) instead of an average value around 6 $a_0$ for the other complexes. This is also very different from the geometry ($R$ = 5.5 $a_0$, $r$ = 1.95 $a_0$ and $\theta$ = 75.0°) and the energy (−30 $cm^{-1}$) calculated by

**Table 1.** Comparison of the well depths and geometries of the He–$N_2$, He–$N_2^+$, He–$CH^+$ and He–HF van der Waals complexes.

| Systems | $R(a_0)$ | $r(a_0)$ | $D_e(\mathrm{cm}^{-1})$ | Method |
|---|---|---|---|---|
| $N_2$ $(\theta = 0°)$ | 7.50 | 2.0743 | −16.197 | |
| $N_2$ $(\theta = 90°)$ | 6.45 | 2.0743 | −21.711 | BCCD(T) |
| $N_2^+(\theta = 0°)$ | 6.80 | 2.11 | −71.08 | |
| $N_2^+$ $(\theta = 90°)$ | 6.08 | 2.11 | −84.459 | CCSD(T) |
| $CH^+$ $(\theta = 0°)$ | 6.09 | 2.13728 | −174.8 | |
| $CH^+$ $(\theta = 86°)$ | 4.10 | 2.13128 | −513.573 | BCCD(T) |
| $CH^+(\theta = 180°)$ | 6.25 | 2.13728 | −66.2 | |
| HF $(\theta = 0°)$ | 5.95 | 1.7328 | −43.70 | |
| HF $(\theta = 95°)$ | 6.10 | 1.7328 | −16.7532 | BCCD(T) |
| HF $(\theta = 180°)$ | 5.65 | 1.7328 | −25.88 | |

Wagner et al. [21] for the He–CH complex. As a result of this unusual geometry of the complex, we will see that the vibrational quenching cross section is surprisingly large.

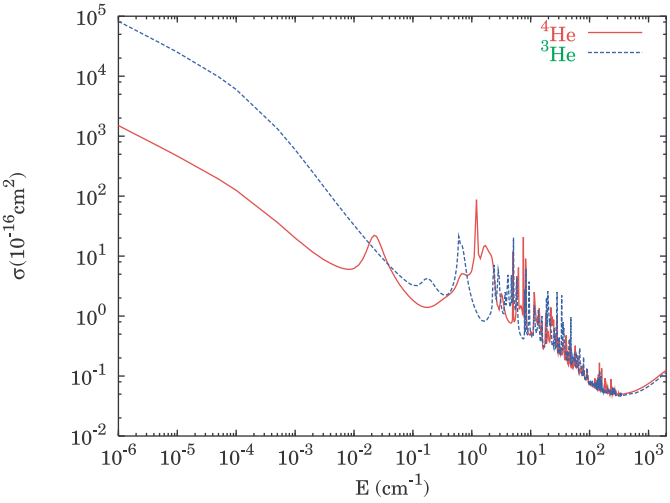


**Fig. 2.** (Color online) Comparison between the quenching cross sections (in $Å^2$) of $CH^+$ ($\nu = 1$, $j = 0$) by collision with $^3$He and $^4$He as a function of the kinetic energy in $\mathrm{cm}^{-1}$.

## 3 Scattering calculations

The Close Coupling scattering equations were propagated in the spaced fixed coordinates using our code Newmat described in previous publications [22]. This program uses the Magnus propagator introduced by Light and coworkers as described in reference [23]. The $T$ matrix elements obtained were used to calculate the cross section for a given transition from an initial vibrational-rotational level labeled by the quantum numbers $\nu j$ to a final level labeled by the quantum numbers $\nu' j'$:

$$\sigma_{\nu j\to\nu' j'}(E_{\nu j}) = \frac{\pi}{(2j+1)\,k_{\nu j}^2} \times \sum_{J=0}^{\infty}(2J+1)\sum_{l=|J-j|}^{|J+j|}\sum_{l'=|J-j'|}^{|J+j'|}\left|T^J_{\nu j,\nu' j'}\right|^2 \quad (2)$$

where $J$ and $l$ are respectively the total and the orbital angular momentum quantum numbers. The wave vector is defined by $k_{\nu j}^2 = \frac{2\mu}{\hbar^2}[E - \varepsilon_{\nu j}]$, $\varepsilon_{\nu j}$ being the eigen energy of the initial rovibrational state $\nu j$, $E$ the total energy, $\mu$ the relative mass of the system and $E_{\nu j} = \frac{\hbar^2 k_{\nu j}^2}{2\mu}$.

As the rotational constant of $CH^+$ ($B \cong 14$ $\mathrm{cm}^{-1}$) is quite large, we needed to include only 10 rotational states in the basis set for each of the two vibrational levels $\nu = 0$ and $\nu = 1$ considered in the calculations. The maximum propagation distance was 1000 Bohr and convergence was checked as a function of the propagator step size. At each point of the propagation grid the matrix elements of the potential were obtained by expanding the potential in Legendre polynomials retaining terms up to $l = 6$ on a grid of 10 points used to calculate the Gauss Hermite quadrature of the vibrational part of the integral. We calculated the diatomic wave function using the same numerical procedure as in any of our previous works.

We now turn to the limit of zero kinetic energy. The effective range is infinite in the case of a charge induced dipole potential. It is however still possible to define the scattering length [24]

$$a_{\nu j} = \alpha_{\nu j} - i\beta_{\nu j} = -\lim_{k_{\nu j}\to 0}\left[\frac{S_{\nu j,\nu j} - 1}{2ik_{\nu j}}\right] \quad (3)$$

where $S_{\nu j,\nu j}$ is an element of the $S$ matrix. This expression is used in the next section to obtain both its real and imaginary parts.

## 4 Results and discussion

Cross sections for elastic scattering and rotationally and vibrationally inelastic scattering were computed for kinetic energy in the range $[10^{-6}; 2000]$ in $\mathrm{cm}^{-1}$. For each value of the kinetic energy the convergence of the cross section was checked as a function of the total angular momentum. The maximum value of total angular momentum $J$ used in the calculations was $J = 80$. Figure 2 shows the comparison of the quenching cross sections of $CH^+$ ($\nu = 1$, $j = 0$) by collision with $^3$He and $^4$He as a function of the kinetic energy. As noticed in previous studies dedicated to ionic systems [25], the long range potential shifts the Wigner regime to lower energies. The width of the intermediate region where the cross section exhibits oscillations here is quite large as it extends up to the Van der Waals well depth (520 $\mathrm{cm}^{-1}$). These oscillations are the signature of the resonances supported by the interaction potential. The nature of these oscillations has been the subject of many recent studies. Here, we find both shape and Feshbach resonances. As can be seen on this figure we obtain a strong isotope effect in the very low kinetic energy regime as the quenching cross sections involving $^3$He are two orders of magnitude larger than their $^4$He counterparts. The same effect and in the same order

**Table 2.** Real and imaginary parts of the scattering lengths associated with the quenching of $CH^+$ ($\nu = 1$, $j = 0$) and $N_2^+$ ($\nu = 1$, $j = 0$) in collisions with the two isotopes of the helium atom.

| | $^3He + N_2^+$ | $^4He + N_2^+$ | $^3He + CH^+$ | $^4He + CH^+$ |
|---|---|---|---|---|
| $\alpha_{\nu=1j=0}$ (Å) | −96.7 | 40.5 | 188.31 | −63.46 |
| $\beta_{\nu=1j=0}$ (Å) | $1.22\times10^{-3}$ | $1.4\times10^{-4}$ | 16.11 | 1.77 |

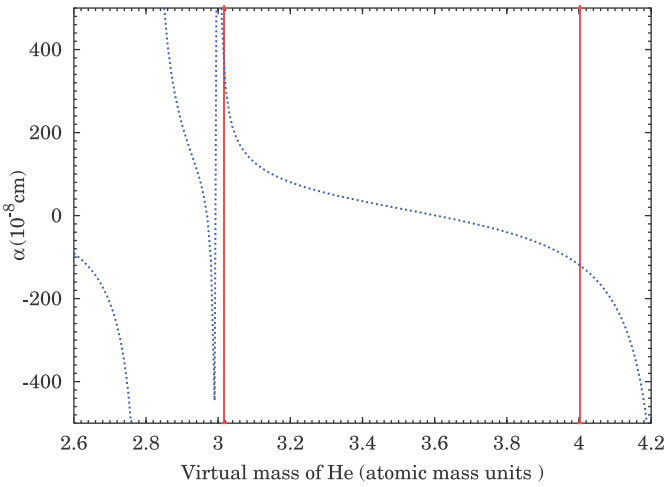


**Fig. 3.** (Color online) Variation of the real part of the scattering length associated with the ($\nu = 1$, $j = 0$) state of $CH^+$ in collisions with a fictitious He atom of variable mass. The vertical bars show the limits corresponding to the two isotopes of He.

was obtained in a previous study dedicated to the He–$N_2^+$ collision (see Fig. 2 of Ref. [8]). We put in Table 2 the real and the imaginary parts of the scattering lengths associated with the quenching of $CH^+(\nu = 1, j = 0)$ and $N_2^+(\nu = 1, j = 0)$ in collisions with the two isotopes of the helium atom. The real part of the scattering length which was found to be large and negative for the $^3$He–$N_2^+$ because of the proximity of a virtual state is large and positive for the $^3$He–$CH^+$ collision showing the existence of a quasi bound state. In the same way, it is large and negative for the $^4$He–$CH^+$ whereas it was found to be large and positive for the $^4$He–$N_2^+$. As noticed in our previous work, this is in contrast with the collision involving $N_2$. In this case the scattering length is small and does not change sign when one move from $^3$He to $^4$He. This simple analysis confirms that the strong isotope effect obtained at very low kinetic energy for the He–$N_2^+$ and He–$CH^+$ collision is a general feature for collisions involving ionic molecules and is a consequence of the strongly attractive long range potential. In order to further analyse these results we drew in Figure 6 of the same previous paper the variation of the real part of the scattering length associated with the ($\nu = 1$, $j = 0$) state of $N_2^+$ in collisions with a fictitious He atom of variable mass. We showed that two zero energy resonances are crossed when one moves from $^3$He to $^4$He for this system. In the case of the He–$CH^+$ collision, only one zero energy resonance is

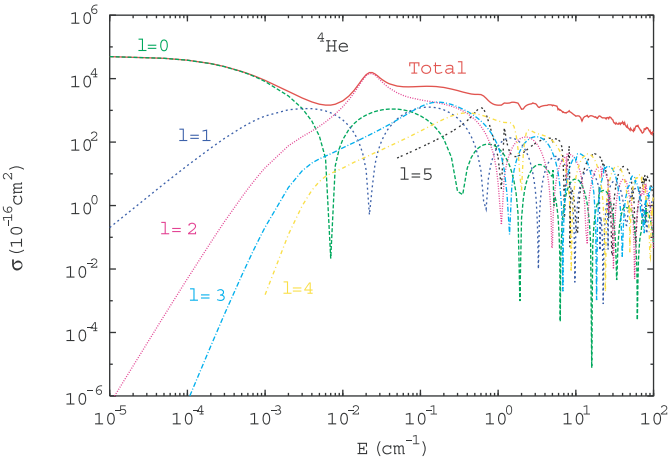


**Fig. 4.** (Color online) Variation of the $l = 0$ to 5 components of the elastic cross sections (in Å$^2$) of $CH^+$ ($\nu = 1$, $j = 0$) in collision with $^4$He as a function of the kinetic energy in cm$^{-1}$.

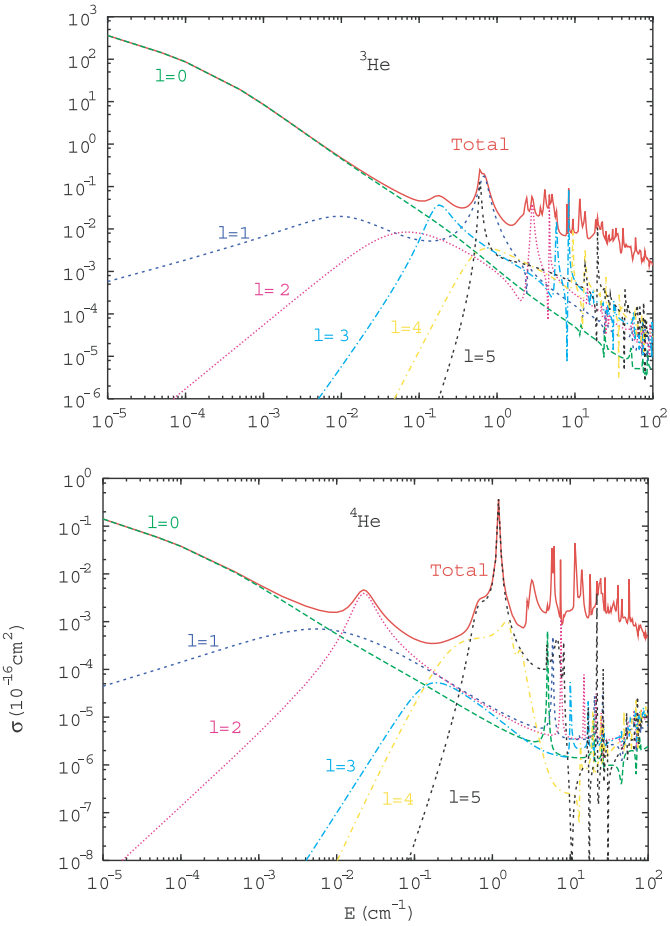


**Fig. 5.** (Color online) Variation of the $l = 0$–5 components of the inelastic cross section (in Å$^2$) for the $CH^+$ ($\nu = 1, j = 0 \Rightarrow \nu = 0, j = 0$) transition in collisions with $^3$He and $^4$He as a function of the kinetic energy in cm$^{-1}$.

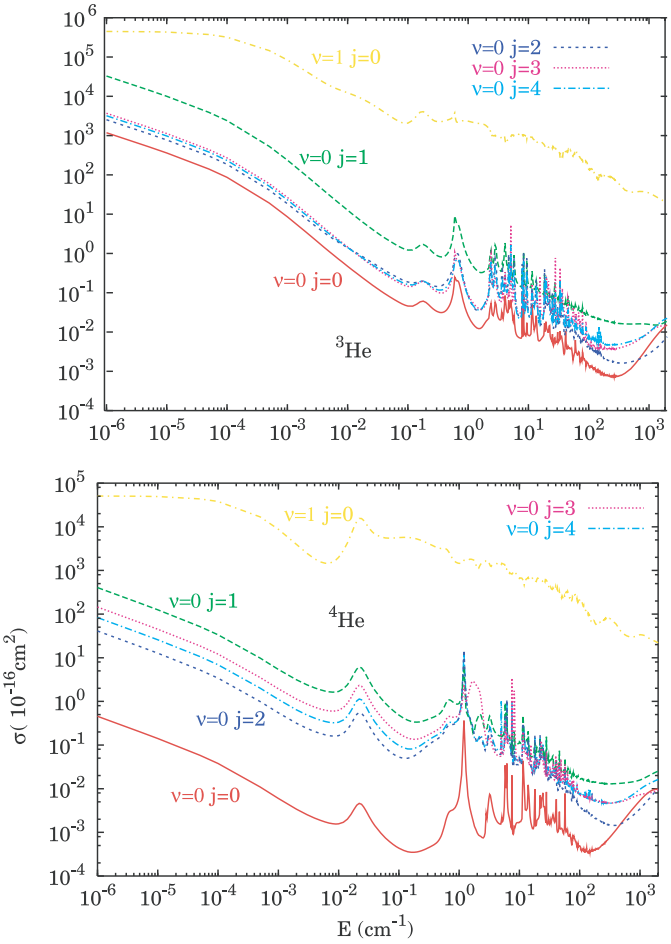


**Fig. 6.** (Color online) Comparison between the cross sections for the elastic and all the deactivation channels (in Å$^2$) of $CH^+$ ($\nu = 1$, $j = 0$) in collisions with $^3He$ and $^4He$ as a function of the kinetic energy in cm$^{-1}$.

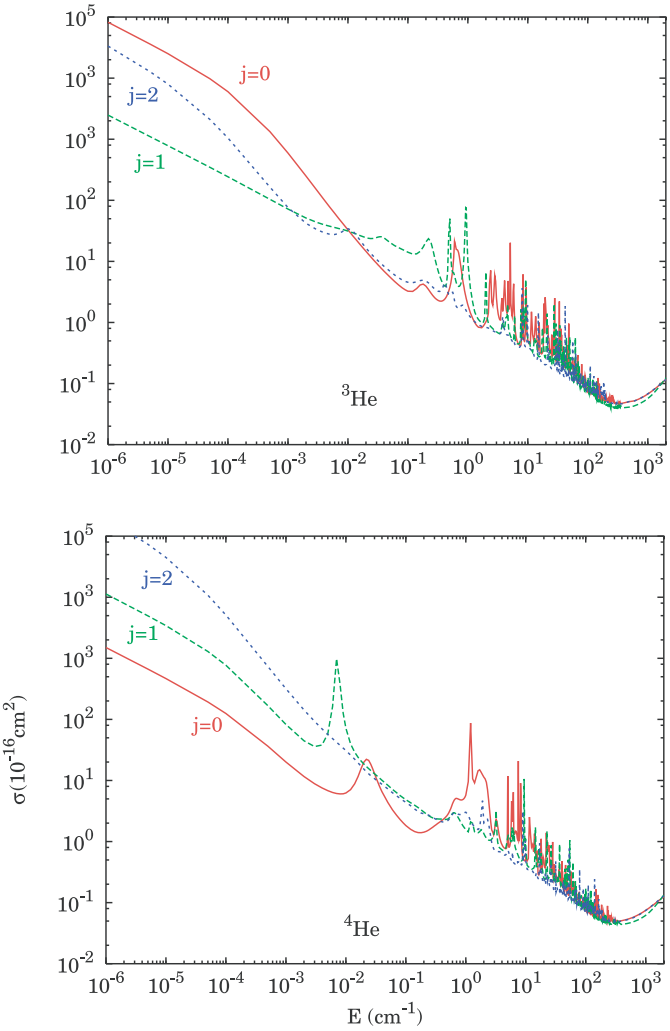


**Fig. 7.** (Color online) Comparison between the vibrational quenching cross sections (in Å$^2$) of $CH^+$ ($\nu = 1$, $j$) for $j = 0$, 1 and 2 by collision with $^3He$ and $^4He$ as a function of the kinetic energy in cm$^{-1}$.

crossed as can be seen in Figure 3 of the present paper. The presence of the virtual state in the case of the $^4He$ + $CH^+$ collision which is associated with the long range charge induced dipole potential is also apparent in Figure 4 where the $s$-wave contribution to the elastic cross section for this collision vanishes around $10^{-2}$ cm$^{-1}$ giving birth to a Ramsauer-Townsend minimum. In Figure 5 the variations of the $l = 0$–5 components of the inelastic cross section for the $CH^+$ ($\nu = 1, j = 0 \Rightarrow \nu = 0, j = 0$) transition in collisions with $^3He$ and $^4He$ are shown as a function of the kinetic energy. The change of relative mass when the collision involves $^3He$ instead of $^4He$ is big enough to change completely the attribution of the partial waves associated with the lowest resonances. This is in contrast with the neutral systems which we analysed previously and is again a consequence of the strength of the long range charge induced dipole potential.

In Figure 6 we compared the cross sections for the elastic and all the deactivation channels of the ($\nu = 1$, $j = 0$) state of $CH^+$ in collisions with the two helium isotopes. The Ramsauer Townsend minimum at $10^{-2}$ cm$^{-1}$ is clearly absent of the elastic channel for the $^3He$–$CH^+$ ($\nu = 1$, $j = 0$) collision. Furthermore, the deactivation towards the ($\nu = 0$, $j = 0$) state is increased by three orders of magnitude when one moves from collision involving $^4He$ to those including $^3He$ whereas the other channels are only increased by two orders of magnitude. In Figure 7, the vibrational deactivation of the $v = 1$, $j = 0$, 1, and 2 states of $CH^+$ in collisions with $^3He$ and $^4He$ are compared. We can first notice that above 1 cm$^{-1}$ the vibrational deactivation of the $\nu = 1$ state is almost independent of the initial rotational state. The resonant character of the vibrational deactivation of the ($\nu = 1$, $j = 0$) state of $CH^+$ in collisions with $^3He$ at very low energy is clearly apparent on this figure as the cross section for the vibrational deactivation of the ($\nu = 1$, $j = 1$) and ($\nu = 1$, $j = 2$) states are smaller whereas they are larger for the collisions involving $^4He$. In Figure 8 the rotational quenching of the $j = 1$ to 5 rotational levels of the fundamental vibrational state of $CH^+$ in collisions with $^3He$ and $^4He$ are compared. For the higher energies the vibrational quenching is as usual

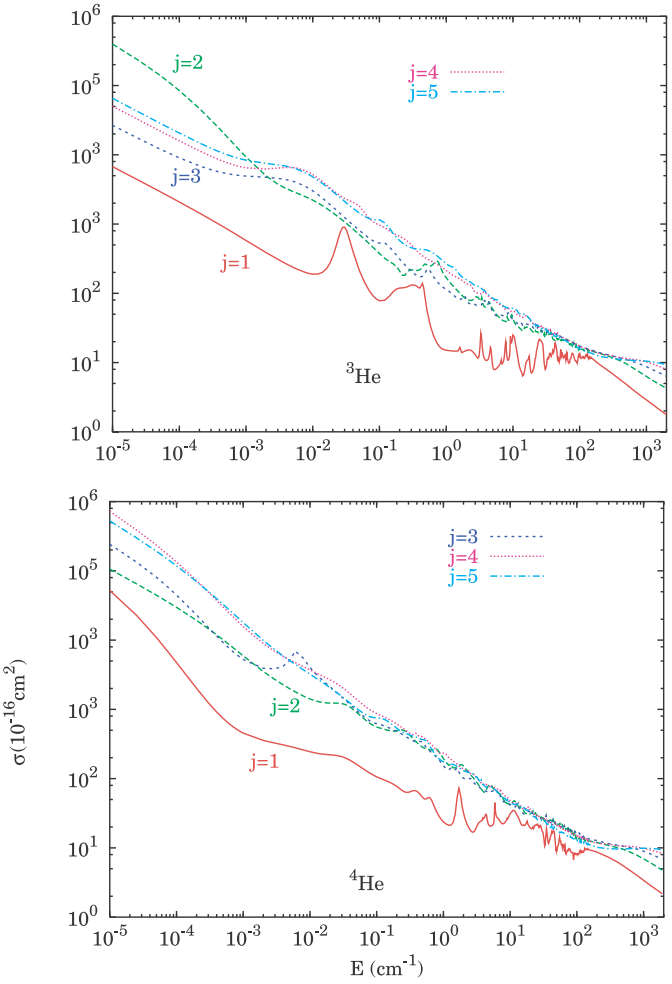


**Fig. 8.** (Color online) Rotational quenching cross sections (in Å$^2$) of $CH^+$ ($\nu = 0$, $j$) by collision with $^3$He and $^4$He as a function of the kinetic energy in cm$^{-1}$.

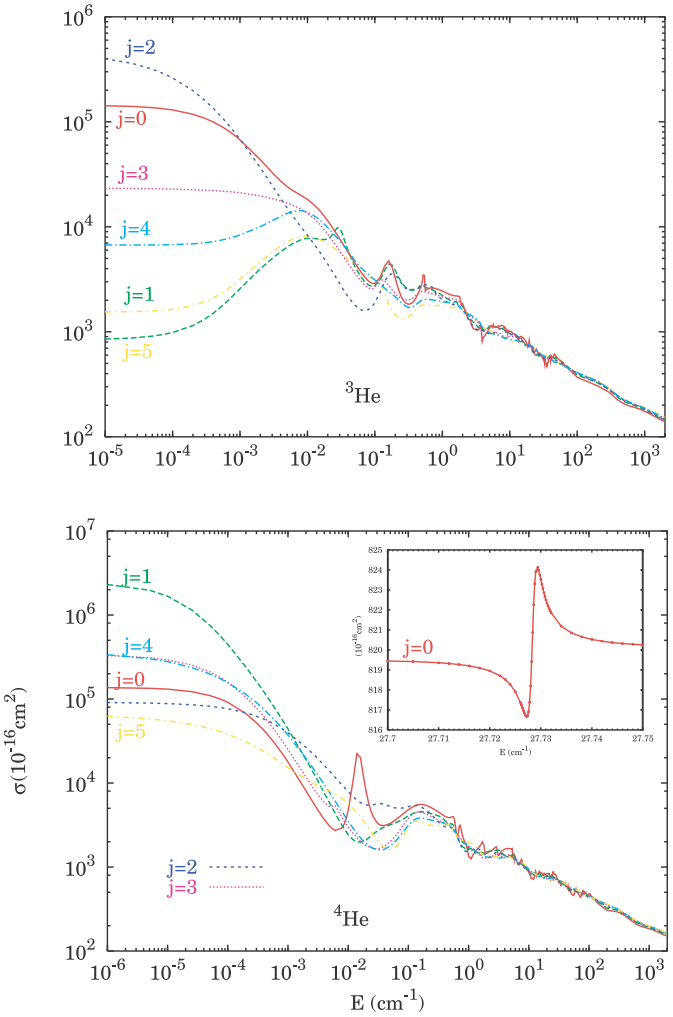


**Fig. 9.** (Color online) Comparison of the elastic cross sections (in Å$^2$) of $CH^+$ ($\nu = 0$, $j$) by collisions with $^3$He and $^4$He as a function of the kinetic energy in cm$^{-1}$. The inset of the panel dedicated to $^4$He shows an enlargement of the $j = 0$ elastic cross section in the region of the opening of the $j = 1$ channel.

between one and two orders of magnitude smaller than the rotational quenching whereas, in the very low energy limit the rotational quenching appears to be of the same order of magnitude than the vibrational deactivation for this system. The long range charge induced dipole potential is known to increase the vibrational deactivation which remains however usually smaller than the rotational quenching. The unusual geometry of the He–$CH^+$ complex discussed above (see Tab. 1) is a possible explanation of this specificity of the He–$CH^+$ collision. A complementary explanation is also possibly the large value of the rotational constant of $CH^+$ which decreases the difference between vibrational and rotational quenching. In general as the rotational level of the molecule increases the energy gap for pure rotational transition also increases and the efficiency of rotational quenching decreases. This is indeed what can be seen in Figure 8 where the rotational quenching does not vary strongly as a function of the rotational level for $j$ greater than 2. On the other hand, the very low collision energy isotope effect already described for the vibrational quenching is here apparent for the rotational quenching of the ($\nu = 0$, $j = 1$) state of $CH^+$. The cross section for the collisions involving $^4$He is larger by two orders of magnitude than the one with $^3$He. This is the reverse of the results obtained for the vibrational quenching. We also represented in Figure 9 the elastic cross sections for the rotational states $j = 0$ to 5 of the fundamental vibrational state $\nu = 0$ of $CH^+$. The $j = 0$ elastic cross sections shown for $^3$He and $^4$He are almost identical at very low collision energy. This is in contrast to what happened for the first vibrationally excited state of $CH^+$. Conversely, there is three orders of magnitude between the very low kinetic energy limits of the $j = 1$ elastic cross sections of $CH^+$ in collisions with $^3$He and $^4$He. The inset of the panel of this figure dedicated to $^4$He shows a Feshbach resonance in the vicinity of the opening of the $\nu = 0$, $j = 1$ level which explains this difference. The change of relative mass when $^4$He is replaced by $^3$He annihilates this effect.

## 5 Conclusion

We presented a detailed study of the vibrational and rotational energy transfer for the He–$CH^+$ collision. A new global 3D potential energy surface was obtained using the RKHS method, by fitting a large grid of ab initio points calculated at the [BCCD(T)] level. The energy of the bent complex is found to be quite large $E = -513.573$ cm$^{-1}$. The large angular anisotropy and the unusually small equilibrium value of the Jacobi $R$ coordinate ($R = 4.1\ a_0$) are two singular features of this system. As a result of these two unusual features, the vibrational quenching cross section is found to be surprisingly large. As for the He–$N_2^+$ collision, we also find a strong isotope effect in the very low collision energy range which was analysed in terms of scattering length. The real part of the scattering length which was found to be large and negative for the $^3$He–$N_2^+$ because of the proximity of a virtual state is large and positive for the $^3$He–$CH^+$ collision showing the existence of a quasi bound state. In the same way, it is large and negative for the $^4$He–$CH^+$ whereas it was found to be large and positive for the $^4$He–$N_2^+$. This effect is due to the strength of the long range charge induced dipole potential and is expected to be a general trend of the collisions involving ionic molecules but may also be encountered for neutral systems with large reduced mass.

## References


1. E. Bodo, F.A. Gianturco, Int. Rev. Phys. Chem. **25**, 313 (2006)
2. J. Doyle, B. Friedrich, R.V. Krems, F. Masnou-Seeuws, Eur. Phys. J. D **31**, 149 (2004)
3. Y.T. van de Meerakker, N. Vanhaecke, G. Meijer, Annu. Rev. Phys. Chem. **57**, 159 (2006)
4. B.C. Sawyer, B.L. Lev, E.R. Hudson, B.K. Stuhl, M. Lara, J.L. Bohn, J. Ye, Phys. Rev. Lett. **98**, 253002 (2007)
5. M. Drewsen, Phys. Rev. Lett. **93**, 243201 (2004)
6. A. Bertelsen, S. Jørgensen, M. Drewsen, J. Phys. B. **39**, L83 (2006)
7. J.P. Shaffer, W. Chalupczak, N.P. Bigelow, Phys. Rev. Lett. **82**, 1124 (1999)
8. T. Stoecklin, A. Voronin, Phys. Rev. A **72**, 042714 (2005)
9. G. Guillon, T. Stoecklin, A. Vorornin, Phys. Rev. A **75**, 052722 (2007)
10. E.E. Feguson, J. Phys. Chem. **90**, 731 (1986)
11. M.H. Alexander, W.R. Kearney, A.F. Wagner, J. Chem. Phys. **100**, 1338 (1994)
12. D.R. Flower, T.S. Monteiro, G. Pineau des Forêts, E. Roueff, in *Rate Coefficients in Astrochemistry*, edited by T.J. Millar, D.A. Williams (Kluwer Academic Publishers, Dordrecht, 1988), pp. 271–280
13. N.C. Handy, J.A. Pople, M. Head-Gordon, K. Raghavachari, G.W. Trucks, Chem. Phys. Lett. **164**, 185 (1989)
14. E. Woon, T.H. Dunning Jr, J. Chem. Phys. **98**, 1358 (1993)
15. F.M. Tao, Y.K. Pan, J. Chem. Phys. **97**, 553 (1992)
16. S.F. Boys, F. Bernardi, Mol. Phys. **19**, 553 (1970)
17. H.-J. Werner, P.J. Knowles, *MOLPRO* version 2000. 1, University of Birmingham, 1999
18. T.S. Ho, H. Rabitz, J. Chem. Phys. **104**, 2584 (1996)
19. T. Stoecklin, A. Voronin, J.C. Rayez, Phys. Rev. A **68**, 032716 (2003)
20. K.P. Huber, G. Herzberg, *Molecular Spectra and Molecular Structure.IY. Constants of Diatomic Molecules* (Van Nostrand, New York, 1987)
21. A.F. Wagner, T.H. Dunning Jr, R.A. Kok, J. Chem. Phys. **100**, 1326 (1993)
22. G. Guillon, T. Stoecklin, Eur. Phys. J. D **39**, 359 (2006)
23. R.W. Anderson, J. Chem. Phys. **77**, 4431 (1982); E.B. Stechel, R.B. Walker, J.C. Light, J. Chem. Phys. **69**, 3518 (1978)
24. R.C. Forrey, N. Balakrishnan, V. Kharchenko, A. Dalgarno, Phys. Rev. A **58**, R2645 (1998)
25. E. Bodo, E. Scifoni, F. Sebastiannelli, F.A. Gianturco, Phys. Rev. Lett. **89**, 283201 (2002)